Multiphosphine-Oxide Hosts for Ultralow-Voltage-Driven True-Blue Thermally Activated Delayed Fluorescence Diodes with External Quantum Efficiency beyond 20%

Jing Zhang, Dongxue Ding, Ying Wei, Fuquan Han, Hui Xu,* and Wei Huang*

Organic light-emitting diodes (OLEDs) of thermally activated delayed fluorescence (TADF) have emerged in recent years, with the feature of harvesting triplet excitons through reverse intersystem crossing (RISC) from the first triplet state (T_1) to the first singlet state (S_1) for 100% internal quantum efficiency.[1–3] The small triplet–singlet splitting (ΔE_{ST}) required for efficient RISC leads to the employment of donor–acceptor (D–A) structure in most of TADF dyes with strong intramolecular charge transfer (ICT), in virtue of their low-energy singlet CT (^{1}CT) states.[4] It is showed that quenching effects are serious for TADF devices due to the involvement of triplet exciton and large-polarity CT states in the electroluminescence (EL) processes.[5–7] Consequently, similar to phosphorescence counterparts, emitters of TADF devices should be dispersed in suitable matrixes to suppress intermolecular interaction induced collisional quenching effects,[6,8] e.g., triplet–triplet annihilation (TTA), singlet–triplet annihilation (STA), and triplet-polaron quenching (TPQ), making TADF host materials crucial for achieving high performance.[9,10]

Although the conventional electrophosphorescent host materials, such as *N,N*′-dicarbazolyl-4,4′-biphenyl (CBP)[2,11] and 1,3-bis(carbazolyl)benzene (*m*CP),[12] are successfully applied in red, green, and sky-blue TADF devices to achieve the external quantum efficiencies (EQE) more than 10%, there are only few host materials competent to blue TADF devices with emission peak around 460 nm and Commission Internationale Ed I'eclairage (CIE) coordinates of $x + y < 0.4$.[3] Bis[4-(9,9-dimethyl-9,10-dihydroacridine) phenyl]sulfone (DMAC-DPS) is one of the best blue TADF dyes, with true-blue emission with peak wavelength at 464 nm and high photoluminescence quantum yield (PLQY) of 80% in toluene and ΔE_{ST} less than 0.1 eV, but the rather high T_1 energy of 2.91 eV.[13] It is known that the T_1 energy of host should be ≈0.2 eV higher than that of dopant to facilitate the efficient positive energy transfer.[14] In this sense, the T_1 value of hosts for DMAC-DPS should reach to 3.1 eV, as for instance bis(2-(di(phenyl)phosphino)-phenyl)ether oxide (DPEPO),[15] which already endowed the state-of-the-art EQE of 19.5% to its DMAC-DPS-based devices.[13,16] However, suffering from the inferiority of DPEPO in carrier injection and transportation, other device properties were not satisfied, such as onset voltage as high as 3.7 V, remarkable EQE roll-offs of 18% at 1000 cd m^{-2} and bathochromic emission peak at 470 nm.[13] Since the high T_1 energy and strong electroactivity always contradict to each other, the lack of high-energy-gap host materials with favorable carrier injecting/transporting ability is the key restraint for realizing the superiority of DMAC-DPS in not only high efficiencies but also low driving voltages and true-blue emission.

The multi-insulating linkage strategy verified by DPEPO is strongly effective in blocking conjugation by thoroughly separating all conjugated units. The employment of insulating linkages with various electroactivities, e.g., electron-donating ether bridge and electron-withdrawing phosphine oxide group, renders the adjustable electrical properties through tuning linkage number and ratio. More significantly, in virtue of multi-insulating linkage, conjugated system can be extended infinitely without reducing excited energy, which makes selective enhancement of electrical performance feasible. In this contribution, as a proof of concept, a tris-phosphine-oxide host material, 2,2′,4-tris(di(phenyl) phosphoryl)-diphenylether (DPETPO, **Figure 1**), was developed to support its DMAC-DPS-based devices with the best results among true-blue TADF diodes reported so far, including the record efficiencies with maxima of 23.0% for EQE and 44.4 lm W^{-1} for power efficiency (PE), the smallest EQE roll-off of 15% at 1000 cd m^{-2}, the lowest onset voltage of 2.8 V and the excellent color purity with emission peak at 464 nm and CIE coordinates of (0.16, 0.21), which were by no means inferior to the best true-blue phosphorescence OLEDs. Besides of their same extremely high T_1 energy of 3.1 eV for effective exciton confinement on DMAC-DPS, in comparison to bi-phosphine oxide DPEPO and tetra-phosphine-oxide 2,2′,4,4′-tetra(di(phenyl) phosphoryl)-diphenylether (DPEQPO), the state-of-the-art device performance of DPETPO is attributed to its remarkably enhanced electroactivity and reduced quenching effects, owing to its enhanced electron affinity, favorable charge mobility and unsymmetrical molecular configuration for intermolecular interplay suppression. This work not only successfully solves the bottleneck of TADF technology in low-voltage-driving efficient blue emission, thereby paving the way toward portable

J. Zhang, D. Ding, Dr. Y. Wei, F. Han, Prof. H. Xu
Key Laboratory of Functional Inorganic Material Chemistry
Ministry of Education and School of Chemistry and Material Science
Heilongjiang University
74 Xuefu Road, Harbin 150080, P. R. China
E-mail: ywei@hlju.edu.cn; hxu@hlju.edu.cn
Dr. Y. Wei, Prof. H. Xu, Prof. W. Huang
Key Laboratory of Flexible Electronics (KLOFE) and Institute of Advanced Materials (IAM)
Jiangsu National Synergistic Innovation Center for Advanced Materials (SICAM)
Nanjing Tech University (NanjingTech)
30 South Puzhu Road, Nanjing 211816, P. R. China

DOI: 10.1002/adma.201502772

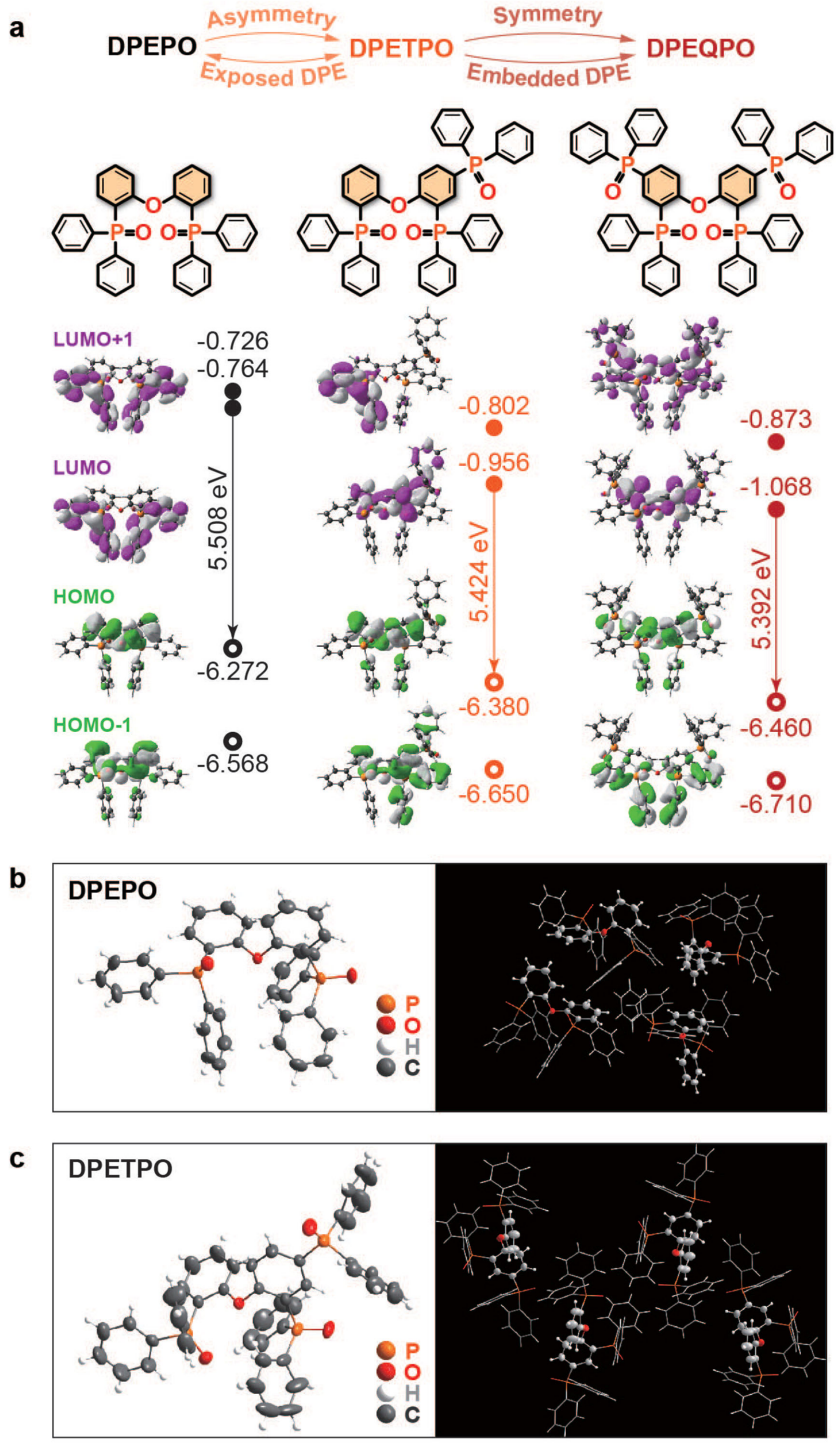

Figure 1. a) Molecular design and energy levels and contours of the frontier molecular orbitals for DPE*x*PO, and single crystal structures and packing diagrams of b) DPEPO, and c) DPETPO. DPPO groups were drawn in tube mode in packing diagrams for clarity.

full-color displays and lighting sources, but also indicates the crucial role of host engineering in developing high-performance TADF diodes for practical applications.

The additional one and two diphenylphosphine oxide (DPPO) groups in DPETPO and DPEQPO were introduced at 4 and 4′ positions of DPE core, using DPEPO as the template (Figure 1a; Scheme S1, Supporting Information). With two DPPOs at 2- and 2′-positions, DPEPO is monosymmetric to render DPE completely exposed to intermolecular interactions (Figure 1b); while the additional DPPO at 4-position in DPETPO breaks the molecular symmetry and partially covers its DPE core, giving rise to the moderate exposure (Figure 1c). But, further incorporation of the fourth DPPO at 4′-position recovers and even enhances the symmetry of DPEQPO, accompanied with the thorough embedment of its DPE core. Despite the various molecular structures, DPEPO, DPETPO, and DPEQPO, collectively named DPE*x*PO, reveal the good thermal stability with temperatures of decomposition (T_d) more than 300 °C (Figure S1 and Table S1, Supporting Information). Their differential scanning calorimetric curves do not contain any distinct glass transitions. Nevertheless, in contrast to DPEPO and DPEQPO, no melting point was observed for DPETPO during cyclic heating, revealing its stable amorphous state and weak intermolecular interactions (inset in Figure S1 and Table S1, Supporting Information). Surface morphologies of their vacuum-evaporated films before and after DMAC-DPS doping are smooth and uniform with root-mean-square roughness less than 0.4 nm (Figure S2 and Table S1, Supporting Information), verifying the improved film formability of DPE*x*PO and the homogeneous dispersion of DMAC-DPS in DPE*x*PO matrixes.

Density function theory (DFT) was utilized to simulate the ground states of DPE*x*PO, figuring out the nature of their electronic characteristics (Figure 1a). The lowest unoccupied molecular orbital (LUMO), the LUMO + 1, the highest occupied molecular orbital (HOMO) and the HOMO-1 of DPEPO with the energy levels of –0.764, –0.726, –6.272, and –6.568 eV (Table S1, Supporting Information) are localized on its DPPO and DPE, respectively. The shallow and separated unoccupied and occupied molecular orbitals (UMO and OMO) of DPEPO are ascribed to the weak electron coupling between electron-withdrawing DPPO and electron-donating DPE at ortho-position. Contrarily, DPPO at 4-position of DPETPO brings about the direct electron coupling with its para-linked DPE. In this case, the inductive effect of P = O in this DPPO makes the LUMO of DPETPO mainly localized on DPE, giving rise to the remarkably reduced LUMO energy level of –2.73 eV; meanwhile, P = O at para-position of phenyl has effect on conjugation extension, rendering the partial contribution of

4-position DPPO to the LUMO of DPETPO. In consideration of the LUMO + 1 location on its 2′-position DPPO and the small LUMO – LUMO + 1 energy gap of 0.15 eV, the whole DPETPO would be involved in electron injection and transportation. In the same way, the HOMO and HOMO–1 of DPETPO with the locations on DPE and 2,4-position DPPOs are reduced to –6.380 and –6.658 eV, respectively. However, the big HOMO – HOMO – 1 energy gap of 0.27 eV suggests DPE as the main hole-transporting channel in DPETPO. It is noteworthy that compared to DPEPO, the LUMO of DPETPO is reduced for 0.19 eV, about two folds of its HOMO reduction (0.11 eV), revealing its enhanced electron injecting ability with relatively small loss of hole injecting ability. In comparison with DPETPO, further incorporating 4′-position DPPO in DPEQPO results in its similar LUMO and HOMO reductions of 0.11 and 0.08 eV, respectively, making it become more unipolar. The DPE-localized LUMO and HOMO, as well as the bigger LUMO – LUMO + 1 and HOMO – HOMO – 1 energy gaps of 0.19 and 0.25 eV, manifest DPE as the main transporting channels for both electron and hole in DPEQPO, which is, however, thoroughly embedded in peripheral DPPOs. Furthermore, besides the exposure degree of carrier transporting channels, ordered molecular arrangement can significantly enhance carrier transportation. According to packing diagrams of their single crystals (Figure 1b,c), both of DPEPO and DPETPO show four types of molecular orientations, which are totally disordered for the former, but two-by-two symmetrical for the latter. In this sense, the molecules in DPETPO films should be more aligned to facilitate carrier transportation.

The experimental LUMO and HOMO energy levels of DPE*x*PO were estimated with cyclic voltammetry (CV, **Figure 2**a). All of the compounds showed two irreversible oxidation peaks with the similar onset voltages around 1.75 V, corresponding to the HOMO energy levels of ≈ –6.53 eV. DPEPO showed a single DPPO-attributed irreversible reduction peak tuned on at –2.30 V, corresponding to the LUMO energy level of –2.48 eV. In addition, one more reduction peaks in the voltammograms of DPETPO and DPEQPO ascribed to their DPE cores were recognized with onset voltages of –2.05 and –1.95 V, corresponding to the LUMO energy of –2.73 and –2.83 eV, which supports the favorable LUMO matching with conventional electron transporting materials, such as 1,3,5-tris(1-phenyl-1H-benzimidazol-2-yl)benzene (TPBi, –2.7 eV) and 4,7-diphenyl-10-phenanthroline (BPhen, –3.0 eV). Therefore, the incorporation of 4 and 4′-position DPPOs in DPETPO and DPEQPO results in the gradual LUMO reductions of 0.25 and 0.10 eV, respectively, as well as the preserved HOMO energy, manifesting the selective and remarkable enhancement of electron injecting abilities of DPETPO and DPEQPO without sacrificing their hole injecting abilities.

The intrinsic carrier transporting abilities of DPE*x*PO were evaluated according to *I*–*V* characteristics of their nominal single-carrier transporting single-layer devices (Figure 2b). DPE*x*PO showed the electron-predominant feature with electron-only current density (*J*) 1–2 orders of magnitude larger than hole-only *J*, which benefits to charge flux balance and recombination zone extension in emissive layers (EML) of conventional *p*-doing devices. As predicted by DFT simulation and single crystal results, DPETPO endowed its devices

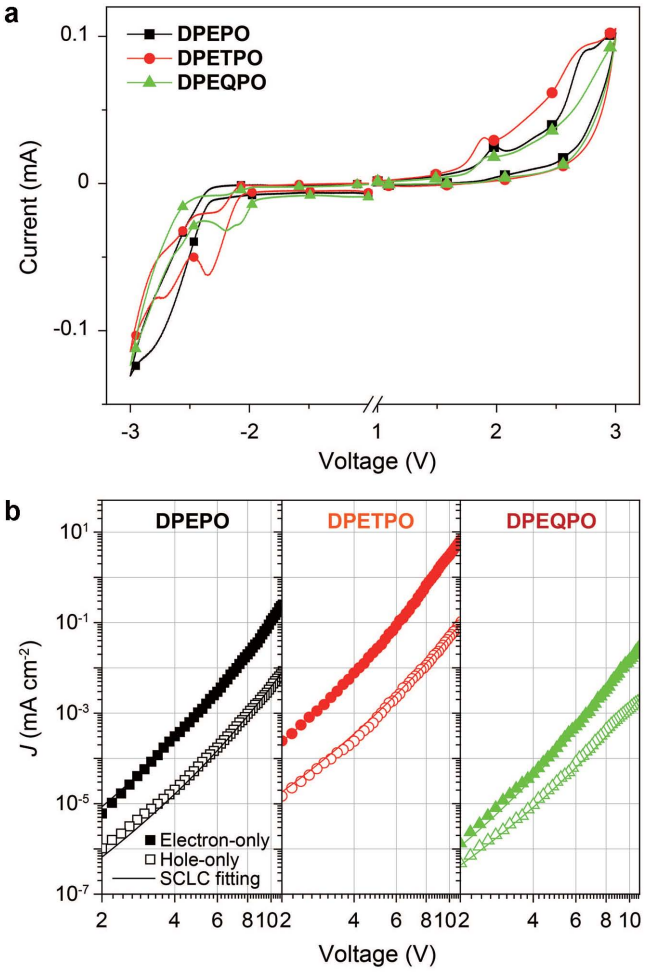

Figure 2. a) Cyclic voltammograms of DPE*x*PO measured at room temperature in CH_2Cl_2 with the scanning rate of 100 mV s^{-1}. b) *I*–*V* characteristics of nominal single-carrier-only devices of DPE*x*PO (solid for electron-only and hollow for hole-only) and the simulated curves according to space-charge-limited-current model.

with the electron and hole mobility of 1.96×10^{-6} and 2.96×10^{-8} cm^2 V^{-1} s^{-1}, which were 1–2 orders of magnitude larger than those of DPEPO and DPEQPO-based devices, respectively (Table S1, Supporting Information). Compared to DPEPO, the improved charge mobility of DPETPO is owing to its enhanced electron affinity, rationally exposed DPE as carrier transporting channel, and regular molecular alignment; while, the reduced mobility of DPEQPO should be mainly attributed to its entirely embedded DPE core. Therefore, when enhancing electroactivity of host materials through multifunctionalization, the exposure of frontier molecular orbital (FMO)-localized groups and regular molecular alignment should be considered, besides of charge affinity.

DPE*x*PO reveal the almost identical optical properties in dilute solutions (10^{-6} mol L^{-1} in CH_2Cl_2, **Figure 3**a). Their electronic absorption spectra consist of three bands around 300, 270, and 230 nm, corresponding to n → p* and p → p* transitions of DPE and p → p* transition of DPPO. In comparison with DPEPO, the extinction coefficients of DPE-attributed transitions for DPETPO

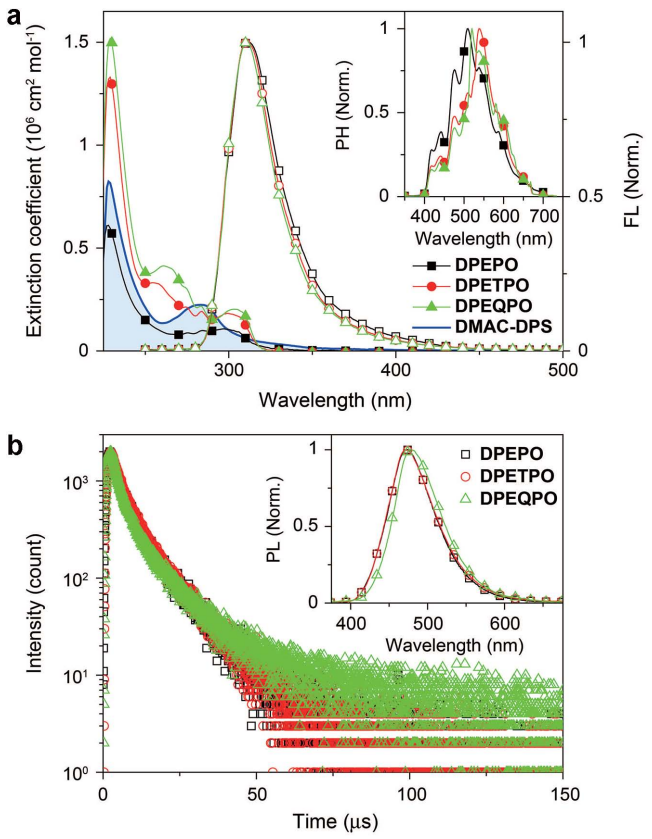

Figure 3. a) Electronic absorption and fluorescence spectra of DPE*x*PO in CH_2Cl_2 (10^{-6} mol L^{-1}) and their time-resolved phosphorescence spectra (inset) measured at 77 K after a delay of 300 ms. b) Transient delay and steady-state emission (inset) spectra of vacuum-evaporated DMAC-DPS-doped DPE*x*PO (10 wt%) films.

are remarkably increased, since the steric hindrance of 4-position DPPO reduces the dihedral angle of DPE core from 86.3° for DPEPO to 70.3° for DPETPO, indicating two more coplanar phenyls in DPE of the latter (Figure 1b,c). The emissions of DPE*x*PO in solutions are almost overlapped with the peak wavelength of ≈310 nm. The visibly and gradually decreased full widths at half maximum from DPEPO, DPETPO to DPEQPO verify the effect of 4 and 4′-substituted DPPOs on suppressing structural relaxation of excited states, owing to the enhanced molecular rigidity. Nevertheless, the small Stokes shifts within 0.1 eV for all of DPE*x*PO reflect their almost consistent ground-state and excited-state configurations and thereby the well-controlled excited-state relaxation. The time-resolved phosphorescence spectra of DPE*x*PO are identical in the range and peak locations (inset in Figure 3a), originated from their similar T_1 locations on DPE cores (Figure S3, Supporting Information). Extremely high T_1 value of 3.10 eV was estimated according to their 0–0 transitions, which can support the effective confinement of triplet exciton on blue TADF dyes, e.g., DMAC-DPS.

Spectral overlapping between emissions of DPE*x*PO and absorption of DMAC-DPS in the range from 275 to 350 nm supports Förster Resonance Energy Transfer from DPE*x*PO to DMAC-DPS, which affords the pure dopant-originated emissions from vacuum-evaporated DPE*x*PO:DMAC-DPS (10 wt%) films with high PLQY more than 80% (inset in Figure 3b; Table S1, Supporting Information). For DPEQPO:DMAC-DPS system, the emission peaked at 478 nm shows a bathochromic shift of 8 nm in contrast to DPEPO and DPETPO-based analogos, which should be ascribed to stabilized CT excited states of DMAC-DPS in more polarized environment provided by DPEQPO with more polar DPPO groups. For the same reason, according to the transient emission spectra, the delay fluorescence lifetime of DMAC-DPS in DPEQPO matrix is

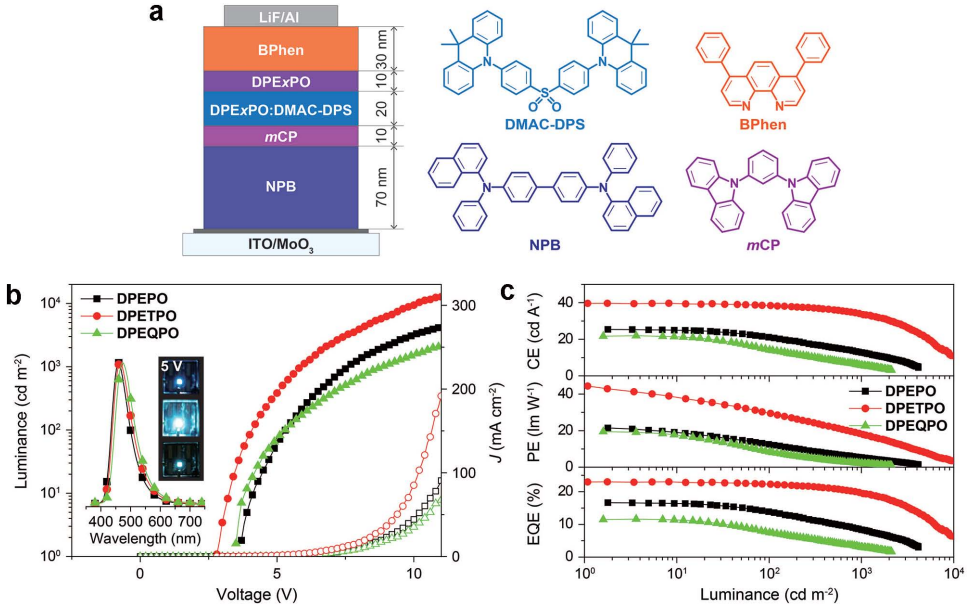

Figure 4. a) Device structure of blue TADF devices and chemical structures of employed materials. b) Luminance–current density (*J*)–voltage characteristics and EL spectra of DPE*x*PO-based blue TADF devices with pictures taken at 5 V (inset). c) Efficiency curves of blue TADF devices for DPE*x*PO related to luminance.

8.9 ms, which is more than 1 ms larger than those of DPEPO and DPETPO-based systems (Figure 3b; Table S1, Supporting Information).

Consequently, on the basis of the moderate density and appropriate spatial distribution of DPPO groups, the electrical performance of DPETPO is dramatically and selectively improved, while its optical properties resemble those of DPEPO, which establishes the basis for constructing highly efficient blue TADF diodes with ultralow driving voltages.

DMAC-DPS-based blue TADF diodes were fabricated with the configuration of ITO|MoO_3 (6 nm)|NPB (70 nm)|*m*CP (10 nm)|DPE*x*PO:DMAC-DPS (10%, 20 nm)|DPE*x*PO (10 nm)|BPhen (30 nm)|LiF (1 nm)|Al, in which MoO_3 and LiF served as hole and electron injecting layers (**Figure 4**a). 4,4′-bis[*N*-(1-naphthyl)-*N*-phenylamino]-1,1′-biphenyl (NPB) and BPhen were adopted as hole-transporting and electron-transporting layers (HTL and ETL), respectively, in virtue of their suitable FMO energy levels and favorable and equivalent charge mobility of $\approx 5 \times 10^{-4}$ cm^2 V^{-1} s^{-1} for facile and balanced carrier transportation (Scheme S2, Supporting Information).[17] Furthermore, in consideration of too low T_1 energy of NPB and BPhen as 2.5 eV, *m*CP, and DPE*x*PO with the T_1 value of 3.0 and 3.1 eV were incorporated as carrier-transporting and exciton-blocking layers to confine excitons in EML of DPE*x*PO : DMAC-DPS.

DPEPO-based devices emitted the pure-blue light with the peak wavelength of 460 nm and favorable CIE coordinates of (0.16, 0.17), which revealed a blueshift of 10 nm in comparison to DPEPO : DMAC-DPS-based devices with TPBi as ETL (inset of Figure 4b and **Table 1**). It is rational that the improved emission color purity can be attributed to the employment of BPhen with stronger electron transporting ability for extending recombination zone and thereby suppressing concentration effect. Likewise, DPETPO endowed the true-blue emission to its devices with the peak wavelength of 464 nm and CIE coordinates of (0.16, 0.21). However, the emission peak of DPEQPO-based devices was at 472 nm, corresponding to sky-blue light with CIE coordinates of (0.17, 0.23), which should be the combined result of the lowest charge mobility of DPEQPO and the strongly polarized environment of DMAC-DPS in DPEQPO matrix.

More excitingly, DPETPO endowed its devices with the ultralow driving voltages of 2.8 V for onset and 4.1 and 5.9 V at practical luminance of 100 and 1000 cd m^{-2} for display and lighting, respectively, which were the lowest values reported so far for the blue TADF devices and comparable to the best results of blue phosphorescent counterparts (Figure 4b and Table 1). The turn-on voltage was even 0.2 V lower than hn/e (2.99 V regarding to the S_1 energy of DMAC-DPS), which was similar to the reported phenomena for the best ultralow-voltage-driven inorganic light-emitting diodes[18] and phosphorescence organic light-emitting diodes (PHOLEDs)[19] with onset voltages about 0.2 V lower than hn/e. It can be attributed to thermal energy *k*T carried by electrons and holes, facilitating carrier diffusion to opposite side for recombination. At the same voltages, DPETPO endowed its devices with the luminance 5–10 folds bigger than those of DPEPO and DPEQPO-based devices. Although the larger electron affinity of DPEQPO rendered the onset voltage of its devices lower than that of DPEPO-based devices, when luminance exceeded 120 cd m^{-2}, DPEPO instead supported the lower driving voltages to its devices. Noticeably, *J* of DPE*x*PO-based devices were exactly in direct proportion to the charge mobility of their hosts, revealing the restrictive effect of host materials on *I*–*V* characteristics of the light-emitting devices. According to energy level diagram of the devices (Scheme S2, Supporting Information), the FMO of DMAC-DPS can perfectly match with those of Bphen and *m*CP to support the almost barrier-free carrier injection, suggesting the direct charge capture and exciton recombination on dopant as predominant EL mechanism. Compared to DPEPO, the correspondence between the most low-lying LUMO of DPEQPO and the reduced onset

Table 1. EL performance of representative blue TADF OLEDs.

Host	Dopant	L_{Max}[a] [cd m^{-2}]	V[b] [V]	h_{Max}[c]	Efficiency roll-offs[d] [%]			CIE	l[e] [nm]	Ref.
					CE	PE	EQE			
–	DMAC-DPS	5970	4.3, –, –	–, –, 19.5	–, –	–, –	–, 25	0.16, 0.28	480	[16]
	DMAC-DPS	16 800	3.0, –, –	–, 29, 14.4	–, –	–, –	–, 19	0.17, 0.30	481	[16]
*m*CP	CzTPN	16 500	4.8, –, –	27.1, 16.7, 11.9	–, –	–, –	–, –	0.17, 0.40	491	[26]
	2CzPN	–	–, –, –	–, –, 13.6	–, –	–, –	–, –	0.17, 0.30	483	[5]
	DCzIPN	<5000	3.5, –, –	–, –, 16.4	–, –	–, –	–, –	0.17, 0.19	462	[27]
DPEPO	CC2BP	3900	4.4	25.5, –, 14.3	–, –	–, –	–, –	0.17, 0.27	484	[28]
	DDCzTrz	<5000	≈4	31.3, 26.2, 18.9	–, –	–, –	–, –	0.16, 0.22	467	[29]
	DtBCz-DPS	–	–, –, –	–, –, 9.9	–, –	–, –	–, –	0.15, 0.07	423	[30]
	DMAC-DPS	>10 000	3.7, –, –	–, –, 19.5	–, –	–, –	–, 18	0.16, 0.20	470	[13]
	DMAC-DPS	<5000	4.6	39.1, 40.9, 22.6	–, 33	–, 56	–, 31	0.16, 0.23	472	[21]
	DMAC-DPS	4135	3.7, 5.4, 7.6	25.3, 21.5, 16.7	18, 50	44, 75	19, 50	0.16, 0.17	460	This work
DPETPO	DMAC-DPS	12 747	2.8, 4.1, 5.9	39.7, 44.4, 23.0	3, 15	34, 60	3, 15	0.16, 0.21	464	This work
DPEQPO	DMAC-DPS	2119	3.5, 5.3, 8.9	22.0, 19.4, 11.6	35, 74	57, 90	35, 74	0.17, 0.23	472	This work

[a]The maximum luminance. [b]Operating voltages for onset, 100 and 1000 cd m^{-2}. [c]The maximum efficiencies of CE (cd A^{-1}), PE (lm W^{-1}), and EQE (%). [d]At 100 and 1000 cd m^{-2}. [e]EL peak wavelength.

voltage of its devices reflected the considerable contribution of DPEQPO to electron injection. Except for charge injection and transportation, the driving voltages of light-emitting devices are defined with specific luminance. Therefore, without the superiority in LUMO energy level to DPEQPO, the lowest driving voltages of DPETPO-based devices in turn were actually ascribed to the largest amount of radiative excitons under these voltages, owing to the superiority of unsymmetrical DPETPO in reducing host-involved interactions for nonradiative transition suppression[20] and/or improved electroactivity for charge flux balance. On account of the large HOMO gaps between *m*CP and DPE*x*PO as ≈0.5 eV, the recombination zones were localized at HTL|EML interfaces at low operation voltages. Along with voltage increasing, high-energy hole can surmount the barrier to enter the HOMOs of DPE*x*PO and thereby generate host-localized excitons, making host-dopant energy transfer considerable in EL process.

The maximum efficiencies of DPEPO-based devices reached to 25.3 cd A^{-1} for current efficiency (CE), 21.5 lm W^{-1} for PE and 16.7% for EQE (Figure 4c and Table 1), which were comparable to the previous reports.[13,21] However, at 1000 cd m^{-2}, the efficiencies were sharply reduced to 12.7 cd A^{-1}, 5.3 lm W^{-1}, and 8.4%, corresponding to roll-offs of 50%, 75%, and 50%, respectively. DPEQPO-based devices achieved the similar maximum efficiencies of 22.0 cd A^{-1}, 19.4 lm W^{-1}, and 11.6%, but accompanied with even more serious roll-offs of 74%, 90%, and 74% at 1000 cd m^{-2}, respectively. Inspiringly, without any additional outcoupling enhancement, the device efficiencies can be dramatically improved to 39.7 cd A^{-1}, 44.4 lm W^{-1}, and 23.0% through utilizing DPETPO as host, which were not only the record values of the true-blue TADF devices to date, but also outstanding in comparison to the best true-blue PHOLEDs.[22] At 100 and 1000 cd m^{-2}, the efficiencies of DPETPO-based devices still remained to be 38.4 cd A^{-1}, 29.4 lm W^{-1}, and 22.3% and 33.4 cd A^{-1}, 17.8 lm W^{-1}, and 19.4%, which correspond to the remarkably reduced roll-offs of 3%, 34%, and 3% at 100 cd m^{-2} and 15%, 60%, and 15% at 1000 cd m^{-2}, respectively. Commonly, the employment of high-energy-gap hosts remarkably increase driving voltages, thereby significantly reducing PE as an indicator of power utilization. Owing to the ultralow driving voltages, the maximum PE of DPETPO-based devices was even higher than their maximum CE, revealing the superiority in energy efficiency. If assistant with additional light extraction technologies, such as micro-len arrays, their PE would be further improved to reach the levels of current commercial light sources, indicating their great potential for practical applications.[23] The almost identical optical properties of DPE*x*PO and the uniform DMAC-DPS dispersion in their films exclude the interference from energy transfer process and dopant-aggregation induced concentration quenching. Despite of EL mechanism featured dopant-predominant charge capture and exciton recombination, the huge differences between EL performances of DPE*x*PO-based devices indeed reflect the crucial effects of host matrixes in TADF diodes. In this case, the state-of-the-art efficiencies and reduced efficiency roll-offs of DPETPO-based devices should be mainly attributed to the effectively suppressed triplet exciton quenching, owing to the significantly reduced host-involved interactions by unsymmetrical configuration of DPETPO.[9,24] Furthermore, the remarkably improved electron mobility of DPETPO can facilitate carrier flux balance in EMLs with respect to excessive hole in the common devices, which further reduced TPQ-induced efficiency roll-off.[25] In consequence, moderate density and rational spatial distribution of DPPO groups in DPETPO realized through rational host configuration engineering are the origins of its outstanding optoelectronic performance.

Although there were already several blue TADF devices reported with the high efficiencies (Table 1), no devices can achieve performance comprehensively close to the blue phosphorescence counterparts in operation voltages, efficiencies, and emission color purity.[3] Consequently, the employment of DPETPO as host and the optimized device configuration successfully realized the substantial breakthrough about blue TADF devices with the state-of-the-art overall performance, including ultralow onset voltage less than 3 V, extremely high efficiencies beyond 20% and true-blue emission, manifesting DPETPO as the best host material for blue TADF devices reported so far.

In summary, the effectiveness of multi-insulating linkage strategy in selectively enhancing optoelectronic performance of hosts through adjusting functional group density and spatial distribution is successfully verified by a series of multiphosphine oxide materials DPE*x*PO with almost identical optical properties. Compared to DPEPO and DPEQPO with the more exposed and thoroughly embedded DPE cores, respectively, the additional 4-position DPPO in DPETPO renders its highest charge mobility of 1.96×10^{-6} and 2.96×10^{-8} cm^2 V^{-1} S^{-1} for electron and hole, respectively, among DPE*x*PO owing to the rational exposure of its DPE core as carrier transporting channel and the regular molecular alignment, accompanied with the suitable LUMO at −2.73 eV for facile electron injection and the preserved T_1 energy as high as 3.1 eV for effective triplet exciton confinement on DMAC-DPS. DPETPO endowed its DMAC-DPS based devices with the lowest driving voltages with onset of 2.8 V and the highest efficiencies with maxima of 23.0% for EQE and 44.4 lm W^{-1} for PE among true-blue TADF devices, which are more than comparable to those of the best phosphorescent counterparts. Therefore, this work finally demonstrates the great potential of TADF diodes in portable full-color displays and high-quality lighting sources by supplying the last link of high-performance blue-emitting devices. It is noteworthy that all of the key indicators for blue TADF devices are sensitive to host characteristics, revealing the urgency, accuracy, and challenge of host development for making this kind of devices commercially applicable.

Supporting Information

Supporting Information is available from the Wiley Online Library or from the author.

Acknowledgements

J.Z. and D.D. contributed equally to this work. This project was financially supported by NSFC (Grant Nos. 51373050 and 61176020), New Century Excellent Talents Supporting Program of MOE (Grant No. NCET-12-0706), Program for Innovative Research Team in

University (MOE) (Grant No. IRT-1237), Science and Technology Bureau of Heilongjiang Province (Grant Nos. ZD201402 and JC2015002), Education Bureau of Heilongjiang Province (Grant No. 2014CJHB005), and the Fok Ying-Tong Education Foundation for Young Teachers in the Higher Education Institutions of China (Grant No. 141012).

Received: June 9, 2015
Revised: September 21, 2015
Published online: November 20, 2015

[1] a) A. Endo, M. Ogasawara, A. Takahashi, D. Yokoyama, Y. Kato, C. Adachi, *Adv. Mater.* **2009**, *21*, 4802; b) K. Goushi, K. Yoshida, K. Sato, C. Adachi, *Nat. Photonics* **2012**, *6*, 253.

[2] H. Uoyama, K. Goushi, K. Shizu, H. Nomura, C. Adachi, *Nature* **2012**, *492*, 234.

[3] Y. Tao, K. Yuan, T. Chen, P. Xu, H. Li, R. Chen, C. Zheng, L. Zhang, W. Huang, *Adv. Mater.* **2014**, *26*, 7931.

[4] a) M. W. Wolf, K. D. Legg, J. H. Parks, R. E. Brown, L. A. Singer, *J. Am. Chem. Soc.* **1975**, *97*, 4490; b) T. Nakagawa, S.-Y. Ku, K.-T. Wong, C. Adachi, *Chem. Commun.* **2012**, *48*, 9580; c) G. Blasse, D. R. McMillin, *Chem. Phys. Lett.* **1980**, *70*, 1; d) C. E. A. Palmer, D. R. McMillin, *Inorg. Chem.* **1987**, *26*, 3837; e) T. Hofbeck, U. Monkowius, H. Yersin, *J. Am. Chem. Soc.* **2015**, *137*, 399; f) M. J. Leitl, V. A. Krylova, P. I. Djurovich, M. E. Thompson, H. Yersin, *J. Am. Chem. Soc.* **2014**, *136*, 16032.

[5] K. Masui, H. Nakanotani, C. Adachi, *Org. Electron.* **2013**, *14*, 2721.

[6] F. B. Dias, K. N. Bourdakos, V. Jankus, K. C. Moss, K. T. Kamtekar, V. Bhalla, J. Santos, M. R. Bryce, A. P. Monkman, *Adv. Mater.* **2013**, *25*, 3707.

[7] Y. J. Cho, K. S. Yook, J. Y. Lee, *Adv. Mater.* **2014**, *26*, 6642.

[8] a) W. Li, Y. Pan, R. Xiao, Q. Peng, S. Zhang, D. Ma, F. Li, F. Shen, Y. Wang, B. Yang, Y. Ma, *Adv. Funct. Mater.* **2014**, *24*, 1609; b) Y. Pan, W. Li, S. Zhang, L. Yao, C. Gu, H. Xu, B. Yang, Y. Ma, *Adv. Opt. Mater.* **2014**, *2*, 510; c) D. Zhang, L. Duan, C. Li, Y. Li, H. Li, D. Zhang, Y. Qiu, *Adv. Mater.* **2014**, *26*, 5050.

[9] C. Han, L. Zhu, J. Li, F. Zhao, Z. Zhang, H. Xu, Z. Deng, D. Ma, P. Yan, *Adv. Mater.* **2014**, *26*, 7070.

[10] C. Han, F. Zhao, Z. Zhang, L. Zhu, H. Xu, J. Li, D. Ma, P. Yan, *Chem. Mater.* **2013**, *25*, 4966.

[11] X. Liu, T. Zhang, T. Ni, N. Jiang, Z. Liu, Z. Bian, Z. Lu, C. Huang, *Adv. Funct. Mater.* **2014**, *24*, 5385.

[12] H. Wang, L. Xie, Q. Peng, L. Meng, Y. Wang, Y. Yi, P. Wang, *Adv. Mater.* **2014**, *26*, 5198.

[13] Q. Zhang, B. Li, S. Huang, H. Nomura, H. Tanaka, C. Adachi, *Nat. Photonics* **2014**, *8*, 326.

[14] S. K. Lower, M. A. El-Sayed, *Chem. Rev.* **1966**, *66*, 199.

[15] C. Han, Y. Zhao, H. Xu, J. Chen, Z. Deng, D. Ma, Q. Li, P. Yan, *Chem. Eur. J.* **2011**, *17*, 5800.

[16] Q. Zhang, D. Tsang, H. Kuwabara, Y. Hatae, B. Li, T. Takahashi, S. Y. Lee, T. Yasuda, C. Adachi, *Adv. Mater.* **2015**, *27*, 2096.

[17] J. Lee, N. Chopra, S.-H. Eom, Y. Zheng, J. Xue, F. So, J. Shi, *Appl. Phys. Lett.* **2008**, *93*, 123306.

[18] E. F. Schubert, *Light-Emitting Diodes*, Cambridge University Press, Cambridge **2006**.

[19] S. J. Su, H. Sasabe, Y. J. Pu, K. Nakayama, J. Kido, *Adv. Mater.* **2010**, *22*, 3311.

[20] Z. Zhang, Z. Zhang, D. Ding, Y. Wei, H. Xu, J. Jia, Y. Zhao, K. Pan, W. Huang, *J. Phys. Chem. C* **2014**, *118*, 20559.

[21] W. Song, I. H. Lee, S.-H. Hwang, J. Y. Lee, *Org. Electron.* **2015**, *23*, 138.

[22] K. S. Yook, J. Y. Lee, *Adv. Mater.* **2012**, *24*, 3169.

[23] a) K. Saxena, V. K. Jain, D. S. Mehta, *Opt. Mater.* **2009**, *32*, 221; b) S. Reineke, F. Lindner, G. Schwartz, N. Seidler, K. Walzer, B. Lussem, K. Leo, *Nature* **2009**, *459*, 234.

[24] a) D. Yu, F. Zhao, C. Han, H. Xu, J. Li, Z. Zhang, Z. Deng, D. Ma, P. Yan, *Adv. Mater.* **2012**, *24*, 509; b) M. Kim, J. Y. Lee, *Adv. Funct. Mater.* **2014**, *24*, 4164; c) E. Mondal, W.-Y. Hung, H.-C. Dai, K.-T. Wong, *Adv. Funct. Mater.* **2013**, *23*, 3096.

[25] a) Q. Wang, I. W. H. Oswald, M. R. Perez, H. Jia, B. E. Gnade, M. A. Omary, *Adv. Funct. Mater.* **2013**, *23*, 5420; b) J. Kalinowski, W. Stampor, J. Mecedilzdotyk, M. Cocchi, D. Virgili, V. Fattori, P. Di Marco, *Phys. Rev. B* **2002**, *66*, 235321; c) S. Reineke, K. Walzer, K. Leo, *Phys. Rev. B* **2007**, *75*, 125328.

[26] T. Nishimoto, T. Yasuda, S. Y. Lee, R. Kondo, C. Adachi, *Mater. Horizons* **2014**, *1*, 264.

[27] Y. J. Cho, K. S. Yook, J. Y. Lee, *Sci. Rep.* **2015**, *5*, 7859.

[28] S. Y. Lee, T. Yasuda, Y. S. Yang, Q. Zhang, C. Adachi, *Angew. Chem. Int. Ed.* **2014**, *53*, 6402.

[29] M. Kim, S. K. Jeon, S.-H. Hwang, J. Y. Lee, *Adv. Mater.* **2015**, *27*, 2515.

[30] Q. Zhang, J. Li, K. Shizu, S. Huang, S. Hirata, H. Miyazaki, C. Adachi, *J. Am. Chem. Soc.* **2012**, *134*, 14706.